









## Article

# Chrysin Directing an Enhanced Solubility through the Formation of a Supramolecular Cyclodextrin–Calixarene Drug Delivery System: A Potential Strategy in Antifibrotic Diabetes Therapeutics

Anca Hermenean <sup>1,†</sup> , Eleftheria Dossi <sup>2,†</sup>, Alex Hamilton <sup>3</sup>, Maria Consiglia Trotta <sup>4</sup> , Marina Russo <sup>5,6</sup>, Caterina Claudia Lepre <sup>4,7</sup>, Csilla Sajtos <sup>8</sup>, Ágnes Rusznyák <sup>8,9</sup> , Judit Váradi <sup>10</sup> , Ildikó Bácskay <sup>9,10</sup> , István Budai <sup>11</sup> , Michele D'Amico <sup>4</sup>  and Ferenc Fenyvesi <sup>8,\*</sup> 

- <sup>1</sup> “Aurel Ardelean” Institute of Life Sciences, Vasile Goldis Western University of Arad, 86 Revolutiei, 310414 Arad, Romania; anca.hermenean@gmail.com
  - <sup>2</sup> Centre for Defence Chemistry, Cranfield University, Defence Academy of United Kingdom, Shrivenham, Swindon SN6 8LA, UK; e.dossi@cranfield.ac.uk
  - <sup>3</sup> Biomolecular Sciences Research Centre (BMRC), Department of Biosciences and Chemistry, College of Health, Wellbeing and Life Sciences, Sheffield Hallam University, Howard Street, Sheffield S1 1WB, UK; a.hamilton@shu.ac.uk
  - <sup>4</sup> Department of Experimental Medicine, University of Campania “Luigi Vanvitelli”, 80138 Naples, Italy; mariaconsiglia.trotta2@unicampania.it (M.C.T.); caterinac.lepre@gmail.com (C.C.L.); michele.damico@unicampania.it (M.D.)
  - <sup>5</sup> Doctoral School of National Interest in Public Administration and Innovation for Disability and Social Inclusion, Department of Mental, Physical Health and Preventive Medicine, University of Campania “Luigi Vanvitelli”, 80138 Naples, Italy; marinarusso801@gmail.com
  - <sup>6</sup> School of Pharmacology and Clinical Toxicology, University of Campania “Luigi Vanvitelli”, 80138 Naples, Italy
  - <sup>7</sup> Doctoral School of Translational Medicine, University of Campania “Luigi Vanvitelli”, 80138 Naples, Italy
  - <sup>8</sup> Department of Molecular and Nanopharmaceutics, Faculty of Pharmacy, University of Debrecen, Nagyerdei St. 98, H-4032 Debrecen, Hungary; sajtos.csilla22@gmail.com (C.S.); rusznyak.agnes@eupar.unideb.hu (Á.R.)
  - <sup>9</sup> Institute of Healthcare Industry, University of Debrecen, Egyetem Square 1, H-4032 Debrecen, Hungary; bacskay.ildiko@pharm.unideb.hu
  - <sup>10</sup> Department of Pharmaceutical Technology, Faculty of Pharmacy, University of Debrecen, Nagyerdei St. 98, H-4032 Debrecen, Hungary; varadi.judit@pharm.unideb.hu
  - <sup>11</sup> Faculty of Engineering, University of Debrecen, Ótmető Street 2-4, H-4028 Debrecen, Hungary; budai.istvan@eng.unideb.hu
- \* Correspondence: fenyvesi.ferenc@pharm.unideb.hu; Tel.: +36-52-411-717-54505  
† These authors contributed equally to this work.



**Citation:** Hermenean, A.; Dossi, E.; Hamilton, A.; Trotta, M.C.; Russo, M.; Lepre, C.C.; Sajtos, C.; Rusznyák, Á.; Váradi, J.; Bácskay, I.; et al. Chrysin Directing an Enhanced Solubility through the Formation of a Supramolecular Cyclodextrin–Calixarene Drug Delivery System: A Potential Strategy in Antifibrotic Diabetes Therapeutics. *Pharmaceuticals* **2024**, *17*, 107. <https://doi.org/10.3390/ph17010107>

Academic Editors: Cinzia Anna Ventura and Federica De Gaetano

Received: 26 November 2023  
Revised: 31 December 2023  
Accepted: 8 January 2024  
Published: 12 January 2024



**Copyright:** © 2024 by the authors. Licensee MDPI, Basel, Switzerland. This article is an open access article distributed under the terms and conditions of the Creative Commons Attribution (CC BY) license (<https://creativecommons.org/licenses/by/4.0/>).

**Abstract:** Calixarene 0118 (OTX008) and chrysin (CHR) are promising molecules for the treatment of fibrosis and diabetes complications but require an effective delivery system to overcome their low solubility and bioavailability. Sulfobutylated  $\beta$ -cyclodextrin (SBECD) was evaluated for its ability to increase the solubility of CHR by forming a ternary complex with OTX008. The resulting increase in solubility and the mechanisms of complex formation were identified through phase-solubility studies, while dynamic light-scattering assessed the molecular associations within the CHR-OTX008-SBECD system. Nuclear magnetic resonance, differential scanning calorimetry, and computational studies elucidated the interactions at the molecular level, and cellular assays confirmed the system’s biocompatibility. Combining SBECD with OTX008 enhances CHR solubility more than using SBECD alone by forming water-soluble molecular associates in a ternary complex. This aids in the solubilization and delivery of CHR and OTX008. Structural investigations revealed non-covalent interactions essential to complex formation, which showed no cytotoxicity in hyperglycemic in vitro conditions. A new ternary complex has been formulated to deliver promising antifibrotic agents for diabetic complications, featuring OTX008 as a key structural and pharmacological component.

**Keywords:** OTX008; chrysin; sulfobutylated  $\beta$ -cyclodextrin; ternary complex; solubilization mechanism; molecular simulation; fibrosis

## 1. Introduction

Calixarenes and cyclodextrins are cyclic molecules with synthetic and natural origins, respectively, and they differ in their building blocks [1]. Calixarenes are synthetic cyclic molecules built from phenolic units linked by methylene bridges, which can be made water-soluble with hydrophilic modifications [2], whereas cyclodextrins are naturally occurring water-soluble cyclic oligosaccharides composed of glycosidic units connected by  $\alpha$ -1,4-glucosidic bonds [3].

Both calixarenes and cyclodextrins share the characteristic of being able to encapsulate guest molecules within their structures, which can enhance the solubility and bioavailability of drugs that are otherwise poorly soluble [2,3]. Specifically, water-soluble calixarenes, like 4-sulphonic calix[n]arenes, have the capacity to increase the solubility of testosterone in water, with effectiveness dependent on their ring size [4]. Previous studies have demonstrated that  $\beta$ -cyclodextrins, including sulfobutylated  $\beta$ -cyclodextrin (SBECD), are effective at improving the solubility and permeability of chrysin (CHR) [5].

CHR is a bioflavonoid present in honey and propolis and has limited bioavailability due to its poor water solubility [6]. Recognized for its various therapeutic properties, CHR exhibits anti-inflammatory, anticancer, and antioxidant activities [7,8]. Recent studies have also highlighted its potential antifibrotic effects [9–11].

OTX008 has the capability to bind with biomolecules like proteins and nucleic acids, influencing enzyme functions [12]. It exhibits anticancer properties by suppressing cancer cell growth and tumor angiogenesis [13]. Zucchetti et al. observed that OTX008, a galectin-1 (Gal-1) targeting compound, can inhibit endothelial cell activities, including proliferation and motility [14]. Additionally, OTX008 has been found to inhibit the overproduction of Gal-1, a protein abundant in the kidneys of diabetic mice and a significant contributor to fibrosis in diabetes [15]. By inhibiting Gal-1 accumulation, OTX008 showcases itself as a new therapeutic inhibitor of Gal-1, aiming to address fibrosis in diabetes.

Even if both OTX008 and CHR are promising molecules for the treatment of fibrosis acting on different targets, they have limited absorption and poor water solubility, and thus, a suitable drug delivery system (DDS) is required for their combined therapeutic application. The common formulation and delivery of the water-insoluble flavonoid CHR and calixarene OTX008 have not been reported yet. Therefore, the aim of the research was to investigate their joint delivery by the subsequent strategy.

While the molecular interaction between cyclodextrins and CHR is well documented [5], a similar relationship between CHR and OTX008 has not been reported yet. The combined use of calixarenes and cyclodextrins to enhance solubility remains largely unexplored. The water solubility of niclosamide was previously enhanced through the joint use of 4-sulphonato-calix[6]arene and hydroxypropyl- $\beta$ -cyclodextrin [16]. Considering OTX008's small cavity and limited water solubility, a weak interaction with CHR was anticipated.

Our strategy entailed employing SBECD to improve the solubility of OTX008, enhancing its drug delivery capabilities.

We aimed to assess the ability of these macrocycles, both individually and in combination, to complex with CHR, forming an advanced DDS. This involved analyzing the phase-solubility of CHR with SBECD in binary arrangements as well as the phase-solubility in ternary systems involving CHR with OTX008 + SBECD. The molecular structures of these compounds are presented in Figure 1.

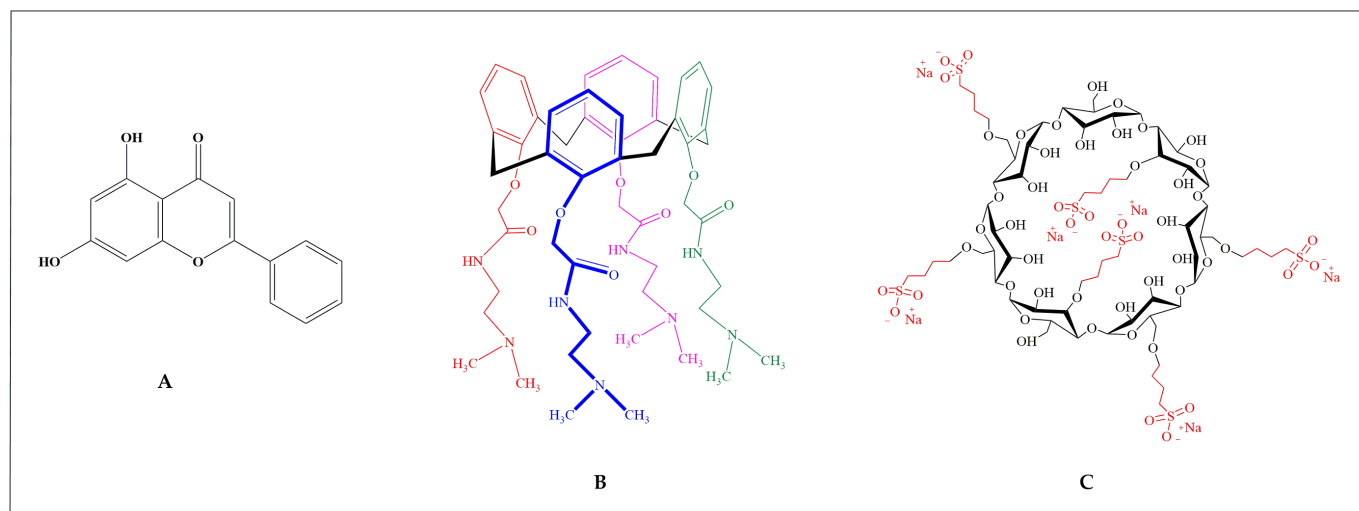


**Figure 1.** Chemical structures of (A) CHR, (B) OTX008, and (C) SBECD.

The selection of SBECD was based on its anionic nature. Given their structural attributes, we anticipated the formation of supramolecular complexes through the interactions of OTX008 and anionic SBECD with CHR, mediated by non-covalent bonds. To examine this hypothesis, we measured the size distribution of the water-based complexes using dynamic light scattering (DLS). We conducted chemical (NMR) and thermal (DSC) analyses of the individual components and their binary mixtures to understand the interactions within the ternary mix, complemented by molecular modeling.

The synthesized complexes were also subjected to *in vitro* biocompatibility assays using embryonic rat cardiac H9c2 cells in both normal and high-glucose conditions, which established a foundation for their potential use in medical treatments.

## 2. Results

### 2.1. OTX008 Solubilization with SBECD

Due to its low water solubility, OTX008 required the use of SBECD (Figure 1) as a solubilizing agent to reach the therapeutically relevant concentration of 0.75 mg/mL. SBECD proved to be an effective solubilizer; solutions of 7.3 mass/mass concentration (m/m%) SBECD were successful in dissolving OTX008 to the target concentration in water. These solution concentrations were, therefore, utilized for subsequent experiments.

### 2.2. CHR Solubilization in OTX008-SBECD Solution

While CHR (Figure 1) does not dissolve in water, its solubility can be enhanced by cyclodextrins, as previously reported [5]. In this study, we examined the solubility of CHR in the solution of 7.3 m/m% SBECD with and without the addition of 0.75 mg/mL OTX008. We observed a significant increase in CHR solubility in the presence of OTX008 ( $p < 0.0001$ ) when compared to solutions containing only cyclodextrins, as shown in Figure 2.

After clarification, the solutions were lyophilized to yield solid products, which were then reconstituted in a 0.9 m/m% NaCl solution. The lyophilized products dissolved completely in the saline solution, making them suitable for further *in vitro* tests and *in vivo* experimentation with parenteral (intravenous or intraperitoneal) administration. The structures of the lyophilized products are presented in Figure 3.

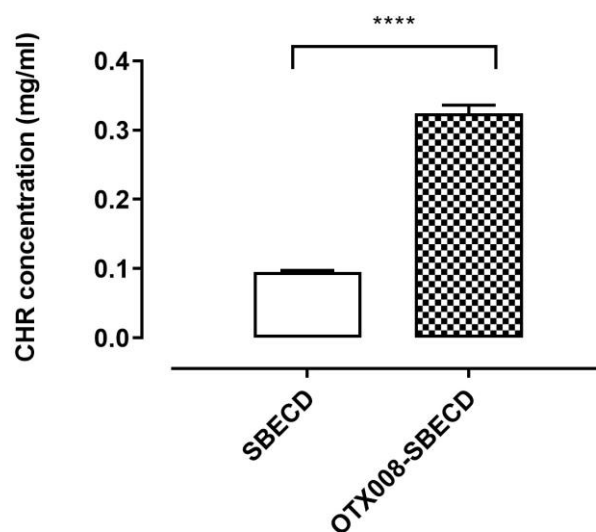


**Figure 2.** CHR is solubilized in water by SBECD (7.3 m/m%) and OTX008-SBECD (OTX008 concentration: 0.75 mg/mL). The simultaneous application of OTX008 and SBECD significantly increased the solubility of CHR compared to SBECD ( $n = 3$ ; \*\*\*\*  $p < 0.0001$ ).

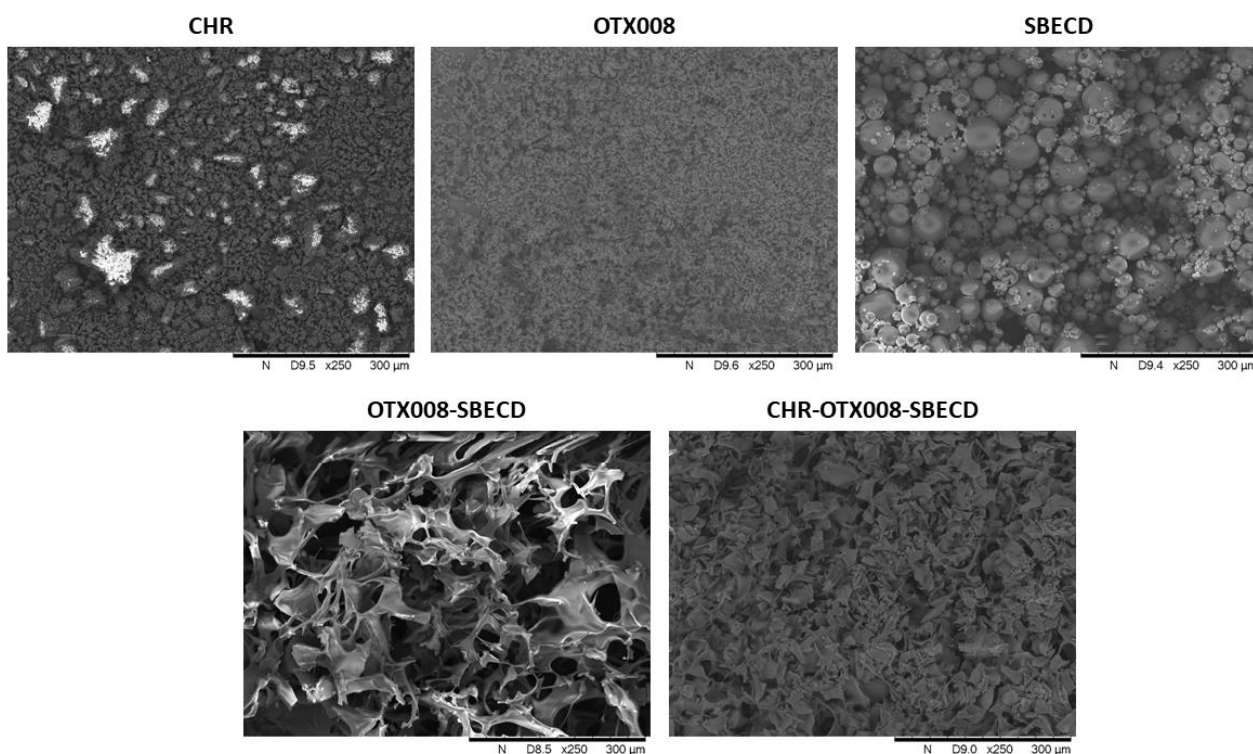


**Figure 3.** Scanning electron microscopic images of CHR, OTX008, SBECD, OTX008-SBECD, and CHR-OTX008-SBECD. Both OTX008-SBECD and CHR-OTX008-SBECD have a porous structure after lyophilization and differ from the pure raw materials. (The white regions show the accumulation of charges on projecting structures).

### 2.3. Phase-Solubility Study

During the phase-solubility analysis, a range of dilutions for SBECD and OTX008-SBECD solutions were employed to dissolve CHR. The solubility of CHR corresponded linearly with the concentrations of SBECD. In contrast, the OTX008-SBECD solutions exhibited non-linear, positively skewed curves, indicating the formation of associations in the solutions (Figure 4).

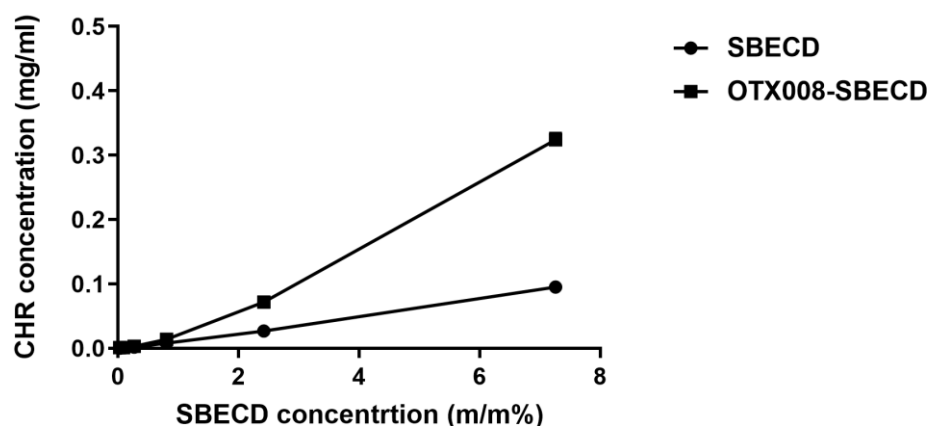


**Figure 4.** Phase-solubility curves of CHR in SBECD and OTX008-SBECD solutions. OTX008 concentration was 0.75 mg/mL in the solutions with the highest SBECD concentrations at 7.3 m/m% SBECD.

#### 2.4. Size Distribution Measurement of the Cyclodextrin Complexes with Dynamic Light Scattering (DLS)

When measured in solution at a concentration of 7.3 m/m%, SBECD displayed molecule associations with a particle size of 351.8 nm as per Dynamic Light Scattering (DLS) data. The particle size was found to increase upon mixing SBECD with OTX008, registering at 1002 nm, and it further escalated significantly higher than 2000 nm (and even higher, whose size range is beyond the detection of the instrument) upon the addition of CHR, forming the ternary CHR-OTX008-SBECD complex (Table 1 and Figure S1).

**Table 1.** Size distribution of SBECD, CHR-SBECD, OTX008-SBECD, and CHR-OTX008-SBECD complexes.

	Peak 1		Peak 2		Peak 3	
	Size	Intensity %	Size	Intensity %	Size	Intensity %
SBECD	351.8 nm	100%	-	-	-	-
CHR-SBECD	1.1 nm	20.8%	94.83 nm	38.1%	3764 nm	41.1%
OTX008-SBECD	1.5 nm	13.2%	1002 nm	86.8%	-	-
CHR-OTX008-SBECD	1.2 nm	24.8%	>2000 nm	>70%	-	-

#### 2.5. pH-Dependent CHR Solubility Determination

The influence of pH on the solubility of CHR, with and without the presence of OTX008, was examined. An increase in pH led to a slight increase in CHR solubility when 7.3 m/m% SBECD was present, as shown in Figure 5.

The initial pH of the 7.3 m/m% SBECD solution was 6.23. Adjusting the pH of the SBECD solution to 8.64 using sodium acetate resulted in a slight improvement in CHR solubility. Conversely, acidifying the OTX008-SBECD solution caused a notable reduction in CHR solubility, aligning it with the levels observed in the SBECD solution alone. Nevertheless, when OTX008 was combined with SBECD in alkaline conditions, CHR solubility was significantly enhanced, increasing three to fourfold. The pH level of the OTX008-SBECD solution was 9.36 when prepared in purified water.

Changing the pH from 3.65 to 9.95 caused only a twofold improvement of CHR's solubility in the presence of SBECD. Both OTX008 and alkalinity are necessary for the significant solubility improvement with SBECD. In the presence of OTX008 and SBECD, the pH changes to 9.36, resulting in a fourfold increase in the solubility of CHR.

Ternary complexes are formed between CHR, OTX008, and SBECD, leading to an increase in the size of molecular associations. The interaction of OTX008 with SBECD and the subsequent formation of a ternary complex are essential for the notable increase in CHR solubility.

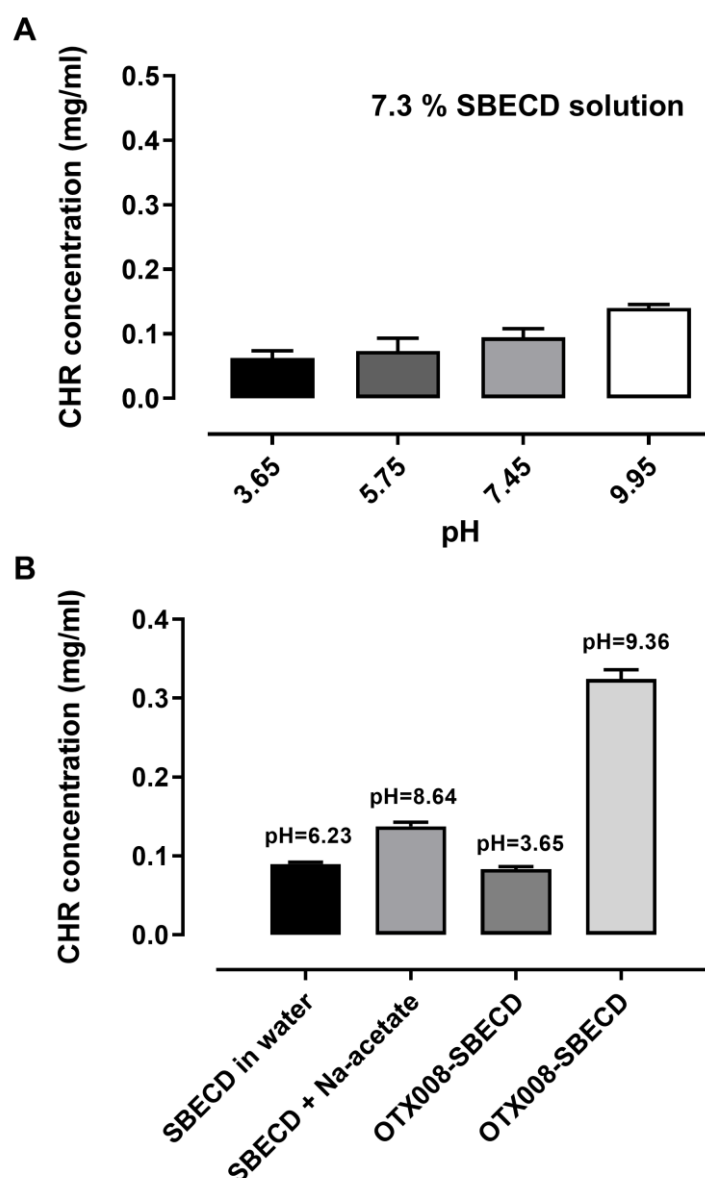


**Figure 5.** pH-dependent solubility of CHR in SBECD solution (A) and in the presence of OTX008 (B). OTX008 increased the pH of the solutions and increased the solubility of CHR.

## 2.6. NMR Studies

To elucidate the reasons behind the enhanced solubility of CHR in the presence of both OTX008 and SBECD,  $^1\text{H}$  and nuclear Overhauser effect spectroscopy (NOESY) NMR spectra of the ternary mixture CHR-OTX008-SBECD, binary mixtures CHR-SBECD and OTX008-SBECD, and single components CHR [17], OTX008, and SBECD were recorded. The ideal deuterated solvent for the spectrometric analysis of all components was DMSO- $d_6$ , while  $\text{D}_2\text{O}$  was used as the best representative of physiological conditions and the evaluation of potential interactions between the components. The spectra of clear solutions of CHR (Figure 6A) and OTX008 (Figure S2) were recorded in DMSO- $d_6$  as a result of their insolubility in  $\text{D}_2\text{O}$ . The SBECD was examined in both deuterated solvents, and when it was in mixtures, it showed the strongest and predominant absorption of the applied magnetic field (Figures S3 and S4) due to its high concentration in the solutions.

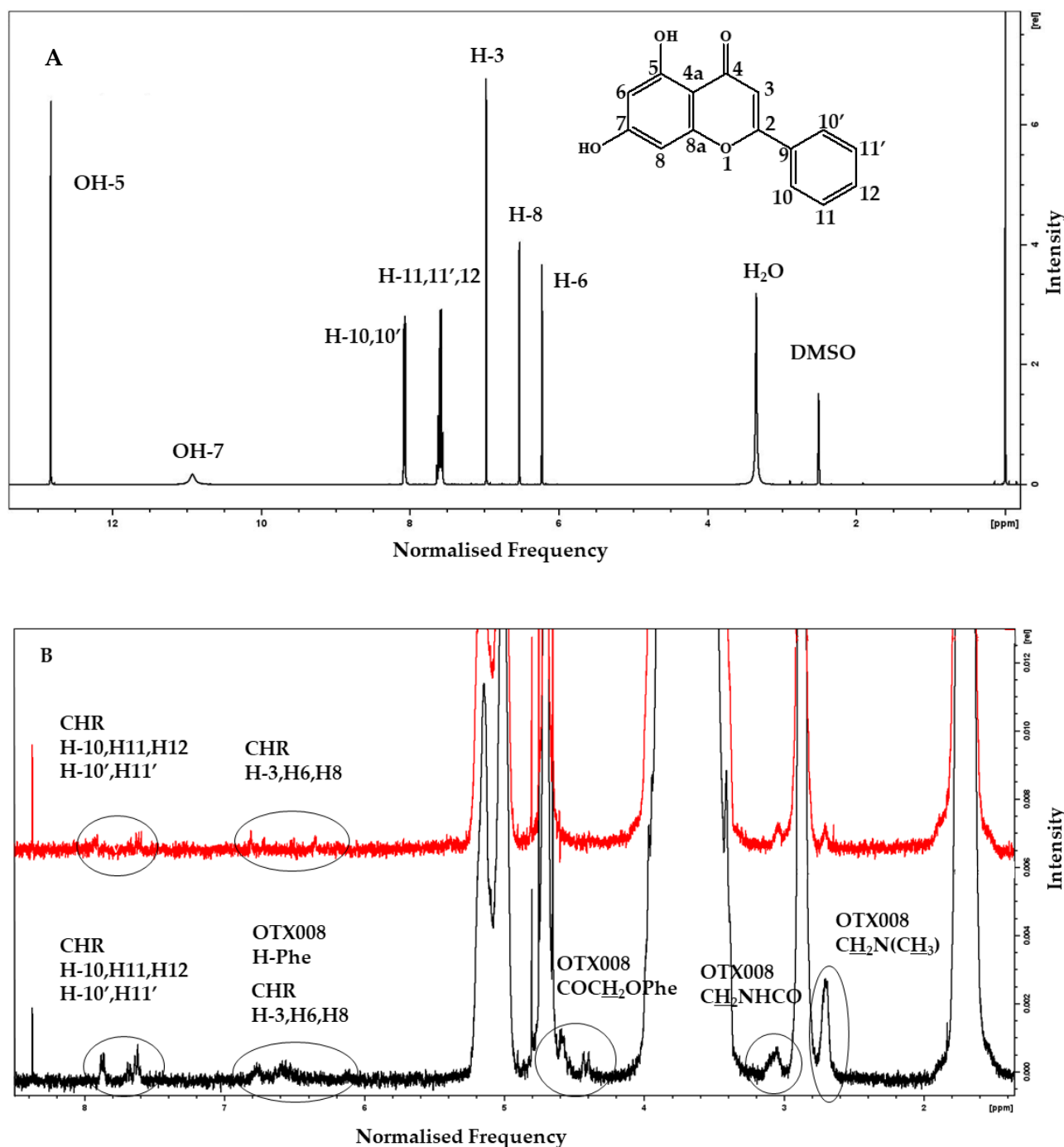


**Figure 6.** (A) Full  $^1\text{H}$  NMR spectrum of CHR in  $\text{DMSO-d}_6$  with assigned peaks. (B)  $^1\text{H}$  NMR spectra of CHR-OTX008-SBECd mixture (black line) and CHR-SBECd mixture (red line) in  $\text{D}_2\text{O}$  showing the presence of CHR and OTX008 (Figure 1) in the ternary structure (framed areas), area 9.0–1.8 ppm. All CHR and OTX008 assignments are extrapolated from their spectra in  $\text{DMSO-d}_6$ . All the unsigned large peaks are associated with SBECd proton absorptions (Figure 1).

### 2.6.1. Binary Mixture of CHR-SBECd

Mixing CHR with SBECd at a molar ratio of 0.01 (CHR/SBECd) in  $\text{DMSO-d}_6$ , as seen in Figure S5, or in  $\text{D}_2\text{O}$ , shown in Figure S6, results in  $^1\text{H}$  NMR spectra that are indistinguishable from those of pure SBECd. This supports the high propensity of CHR to be hosted within the toroidal cavity of the cyclodextrin structure. Such inclusion is consistent with the formation of sizable aggregates detected in DLS studies and is corroborated by the

absence of free CHR signals in the NOESY spectra of the binary mixture, as depicted in Figures S7 and S8.

### 2.6.2. Binary Mixture of OTX008-SBEC

The NMR spectra of the binary mixture, composed at a molar ratio of 0.02 (OTX008/SBEC), display signals corresponding only to SBEC when analyzed in DMSO- $d_6$ , as shown in Figures S9 and S10. This observation is likely due to the chosen molar proportions of the components in the mixture. Interestingly, computational simulations, as outlined in the subsequent paragraph, indicate that the interaction between SBEC and OTX008 is not energetically favored (+0.9 kcal mol<sup>-1</sup>).

### 2.6.3. Ternary Mixture CHR-OTX008-SBEC

When CHR is mixed with SBEC (0.03 mol/mol, CHR/SBEC) and OTX008 (1.6 mol/mol, CHR/OTX008) in DMSO- $d_6$  (Figures S1) or D<sub>2</sub>O (Figure S16), the <sup>1</sup>H NMR spectra of the mixture show some differences in protons' chemical shifts when compared to those observed for the single components of the mixture. In the DMSO- $d_6$  spectra, the signals attributed to the two OHs of the CHR molecule bonded to carbon atoms in the 5 and 7 positions are very weak or even not seen at all (Figure 6A). This can be due to the molar ratio of the CHR in the ternary mixture or because it is involved in the non-bonded interaction that keeps the supramolecular structure together.

No changes were observed for protons bonded to carbon atoms in positions 10 to 10', suggesting that the potential interaction of the CHR with the other two components of the ternary mixture involves the opposite part of the molecule; small chemical shifts to a higher magnetic field of 0.02 ppm, 0.05 ppm, and 0.03 ppm, respectively, for protons H-3, H-8, and H-6, indicating interaction of the condensed part of the CHR (Figures 6A, S13 and S14). The shape of the last three protons is broader, which could imply electrostatic interactions through hydrogen bonding with the two other components (OTX008 and SBEC), which contain several oxygen and/or nitrogen atoms.

In the same spectrum (Figure S11), OTX008 protons bonded to nitrogen atoms (NH) are subjected to a small chemical shift to a higher magnetic field from 8.32 to 8.29 ppm (0.03 ppm). Interestingly, a larger downfield effect from 6.65 ppm to 6.71–6.59 ppm of OTX008 aromatic protons indicated that the upper aromatic cup shape of OTX008 is distorted by the three-member interaction (Figure S14). This is also supported by the broadness of the resulting signal, which is centered at 6.70 ppm. The above observations indicated that the CHR molecules are electrostatically bonded to the carbonyl groups of the OTX008 side arms and are causing this distortion (confirmed by simulations). There were no changes in the chemical shifts of the SBEC protons (Figure S11).

Three signals attributed to CHR aromatic protons H-3, H-8, and H-6 at 6.60 ppm, 6.55 ppm, and 6.22 ppm, respectively, appear in the NOESY spectra of the ternary mixture, confirming that any interaction of CHR with the system involves the phenolic aromatic ring (Figures S15 and S16).

Some small differences (0.05 ppm) in the chemical shifts of the aromatic protons of CHR were observed in spectra recorded in D<sub>2</sub>O when the binary CHR-SBEC and the ternary mixture were compared (Figure 6). Those peaks were broader, indicating a complex new situation in the macrostructure. The NOESY spectra also confirm the presence of free CHR molecules not involved in holding together the CHR-OTX008-SBEC macrostructure (Figure 6).

## 2.7. Thermal Analysis

The thermal analysis of all components and their binary and ternary mixtures revealed that the properties of all components were affected when mixed (Table S1 and Figures S17 and S18). In the ternary mixture, all components degrade together, with a peak at 300 °C indicating the formation of a unique macrostructure, while those CHR [18]



molecules accommodated in the free volume of the macrostructure kept their thermal identity with a melting point at 290 °C.

### 2.8. Computational Studies on CHR-OTX008-SBECD Interactions

Initial supramolecular structures for the interactions between CHR, OTX008, and SBECD were optimized with the GFN2-xtb quantum semi-empirical method. This method has been previously shown to produce good-quality geometries for a range of species, from small organics to polymers.

To gain a better understanding of the relevant interactions, binding free energies have been calculated with DFT calculations (RI-PBE\_D3BJ/def2-tvzvp level of theory). All starting geometries were taken from the optimized GFN2-xtb structures.

The calculated geometries of optimized binding interactions between all molecular components (OTX008, CHR, SBE, and CD) are shown in Figure 7, with calculated free energies reported in Table 2.

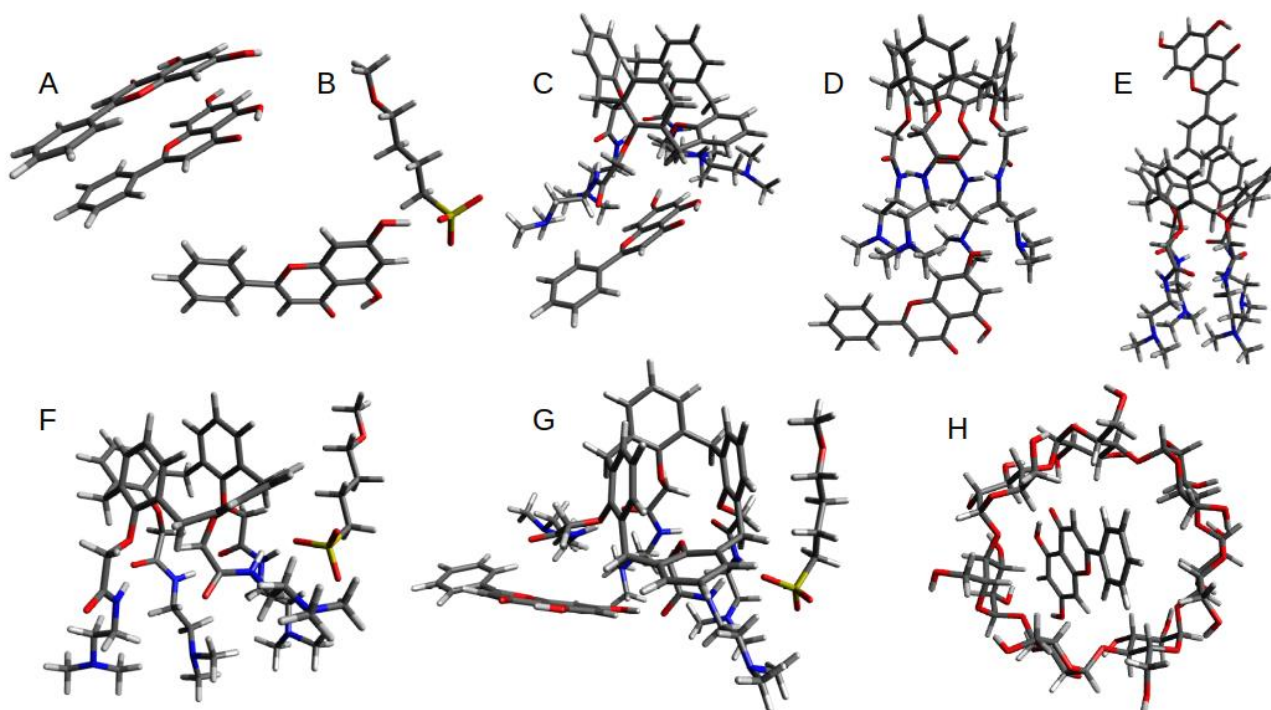


**Figure 7.** The figure shows the DFT-optimized structures evaluated in this study; see Table 2 for calculated binding energies. Structure (A) shows the preferential CHR–CHR dimer alignment, with a binding energy of  $-14.0 \text{ kcal mol}^{-1}$ ; alternative stacked orientations were within  $2 \text{ kcal mol}^{-1}$ , suggesting multiple alignment possibilities. The hydrogen-bonded dimer adducted was calculated to be  $9 \text{ kcal mol}^{-1}$  less favorable. Structure (B) highlights the CHR–SBE interaction, with a strong hydrogen bond between the  $-\text{OH}$  group of the CHR molecule and the  $\text{SO}_3^-$  group of the SBE arm. Structures (C–E) show the possible interactions between CHR and OTX008, with hydrogen bonding between the CHR hydroxyl group and the carbonyl on the OTX008 unit being preferential. Structure (F) shows the most favored interaction between the amine groups of the OTX008 unit and the SBE arm. Structure (G) highlights the tertiary adduct involving CHR–OTX008–SBE; the structure shows a cooperative effect where the OTX008–SBE interaction ( $\text{R-NH}\cdots\text{SO}_3\text{-R}$ ) facilitates the OTX008–CHR interaction ( $\text{R-CO}\cdots\text{HO-R}$ ). This compensates for the increased entropic contribution of the tertiary complex. Structure (H) shows the host–guest binding of the CHR in the CD cavity.

**Table 2.** Binding free energies for each interaction. See Figure 7 for the structures.

Structure	Interaction	G <sub>solv</sub> kcal/mol
A	CHR dimer	−14.0
B	SBECD-CHR (arm)	−6.2
C	OTX008-CHR (carbonyl)	−12.6
D	OTX008-CHR (amine)	−10.8
E	OTX008-CHR (calixarene)	−2.7
F	SBECD-OTX008	+0.9
G	SBECD-OTX008-CHR	−8.6
H	SBECD-CHR (cavity)	−4.5

(CHR—Chrysin, SBECD—Sulfobutylated  $\beta$ -cyclodextrin sodium salt).

Given the size and conformation flexibility of the SBECD molecule, full DFT calculations would prove computationally too expensive while also having a significant level of uncertainty with the results. A model system for the binding interaction between SBECD, CHR, and OTX008 was chosen to focus on the  $\text{SO}_3^-$  interactions, as these showed to be preferential in the GFN2-xtb optimization. The GFN2-xtb optimization interactions between SBECD and CHR and OTX008 and SBECD are also presented in Figure S19.

The relative binding energies (Table 2) clearly highlight the preferential binding of the OTX008-CHR interaction via the carbonyl of the amide arms. There is also a reasonably strong interaction between the SBECD and CHR molecules, both with the arms and the cyclodextrin cavity of SBECD. Interestingly, the SBECD-OTX008 interaction is not favorable (+0.9 kcal mol<sup>−1</sup>). This agrees with the reduction in binding energy on the combination of SBECD-OTX008-CHR compared to the initial OTX008-CHR interaction. The formation of CHR dimers is also preferential.

### 2.9. Cell Viability

Exposure to CHR, SBECD, and their combinations with CHR, DMSO, or M did not impair H9c2 cell survival in either normal glucose (NG) or high glucose (HG) mediums. Furthermore, all tested concentrations of OTX008 (2.5, 1.25, and 0.75  $\mu\text{M}$ ), whether alone or in combination with SBECD (OTX008-SBECD), as well as the mixture CHR-SBECD with OTX008 (CHR-OTX008-SBECD), did not diminish cell viability under NG conditions, as depicted in Figure 8A. These concentrations were also non-toxic in the HG medium, as shown in Figure 8B. On the contrary, they lead to a significant improvement in cell viability in H9c2 cells exposed to HG. Notably, OTX008 alone and its combinations with SBECD markedly enhanced cell viability at all three tested doses (as seen in Figure 8C–E). The ternary mixtures of CHR-OTX008-SBECD began to show effectiveness at a 1.25  $\mu\text{M}$  OTX008 concentration, according to Figure 8D. It is particularly interesting that the combination of OTX008-SBECD or CHR-SBECD-OTX008 resulted in the most pronounced increase in cell viability at the highest OTX008 dose of 2.5  $\mu\text{M}$ , as illustrated in Figure 8C.

### 2.10. Reactive Oxygen Species (ROS)

Exposure to CHR, SBECD, and their combinations with CHR, DMSO, or M did not affect ROS levels in either NG or HG conditions (Figure 9A). As expected, H9c2 cell growth in the HG medium showed a marked increase in ROS intracellular levels compared to the NG group ( $p < 0.001$ ) (Figure 9B). Furthermore, all tested concentrations of OTX008 (2.5, 1.25, and 0.75  $\mu\text{M}$ ), whether alone or in combination with SBECD (OTX008-SBECD), significantly reduced ROS levels in HG conditions (Figure 9C–E). Notably, the ternary mixtures of CHR-OTX008-SBECD began to show effectiveness at 1.25  $\mu\text{M}$  OTX008 concentration, resulting in the most pronounced decrement of intracellular ROS levels at the highest OTX008 dose of 2.5  $\mu\text{M}$ , as illustrated in Figure 9C.

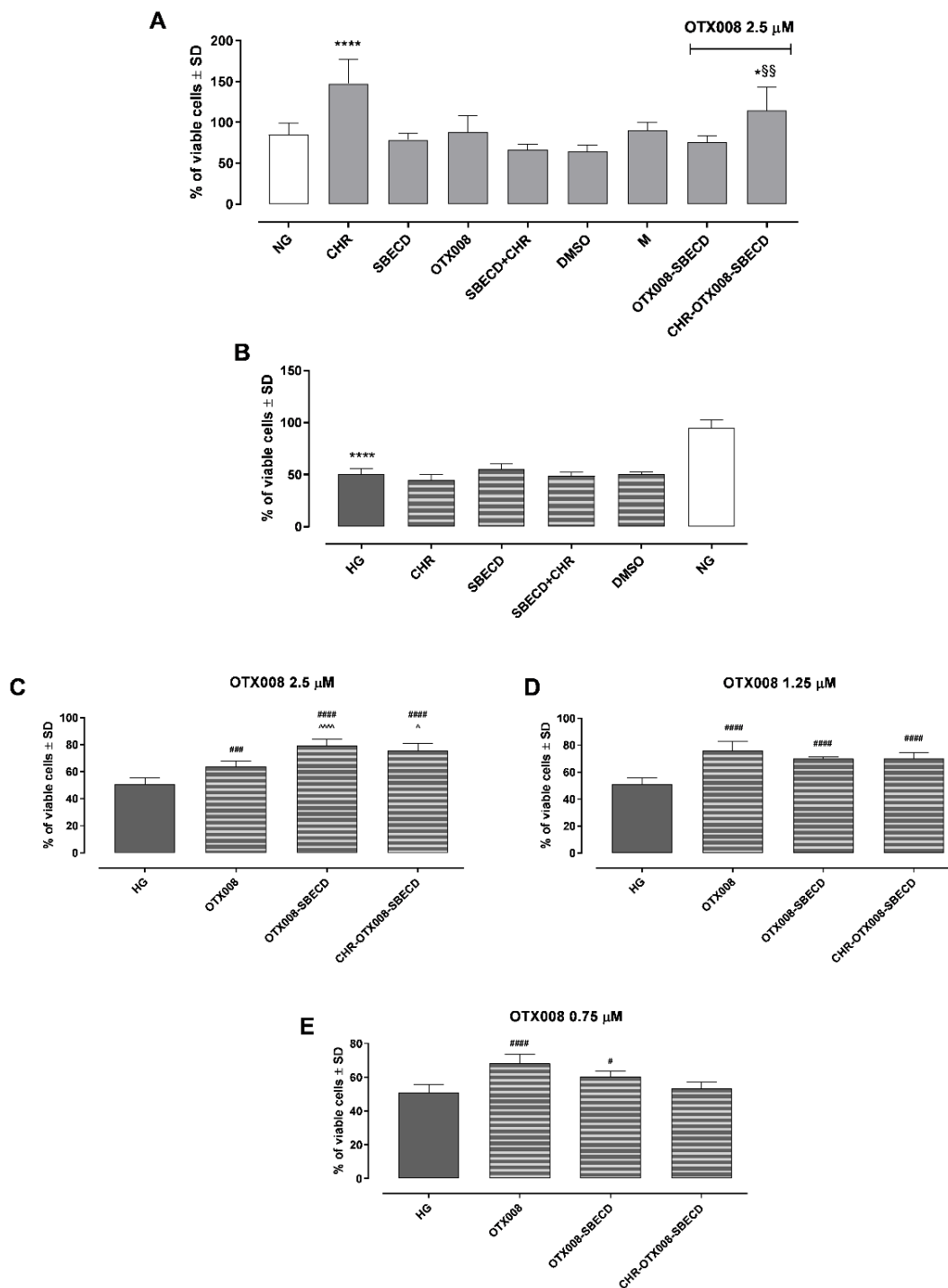


**Figure 8.** H9c2 cell viability after treatment with the compounds in NG (A) and HG (B) conditions (where the NG group is reported as the control). In NG cells, OTX008 was tested at the maximum dose of 2.5 μM. In HG cells, OTX008 was tested at doses of 2.5–1.25–0.75 μM (C,D,E, respectively). Cell viability was determined by the MTT assay and reported as the percentage of cell viability ± SD. NG = 5.5 mM D-glucose; HG = 33 mM D-glucose; CHR = CHR 0.399 mg/mL; SBECD = Sulfobutylated -β-cyclodextrin 7.3 m/m%; SBECD + CHR = SBECD + 0.095 mg/mL CHR; DMSO = dimethyl sulfoxide 2.5%; M = mannitol 27.5 mM; OTX008 = OTX008 (2.5–1.25–0.75 μM); OTX008-SBECD = OTX(2.5–1.25–0.75 μM)-SBECD; CHR-OTX008-SBECD = CHR (0.324 mg/mL)-OTX(2.5–1.25–0.75 μM)-SBECD. \*  $p < 0.05$ , \*\*\*\*  $p < 0.0001$  vs. NG; #  $p < 0.05$ , ###  $p < 0.001$ , ####  $p < 0.0001$  vs. HG; ^  $p < 0.05$ , ^^^  $p < 0.0001$  vs. OTX008; §§  $p < 0.01$  vs. OTX008-SBECD.

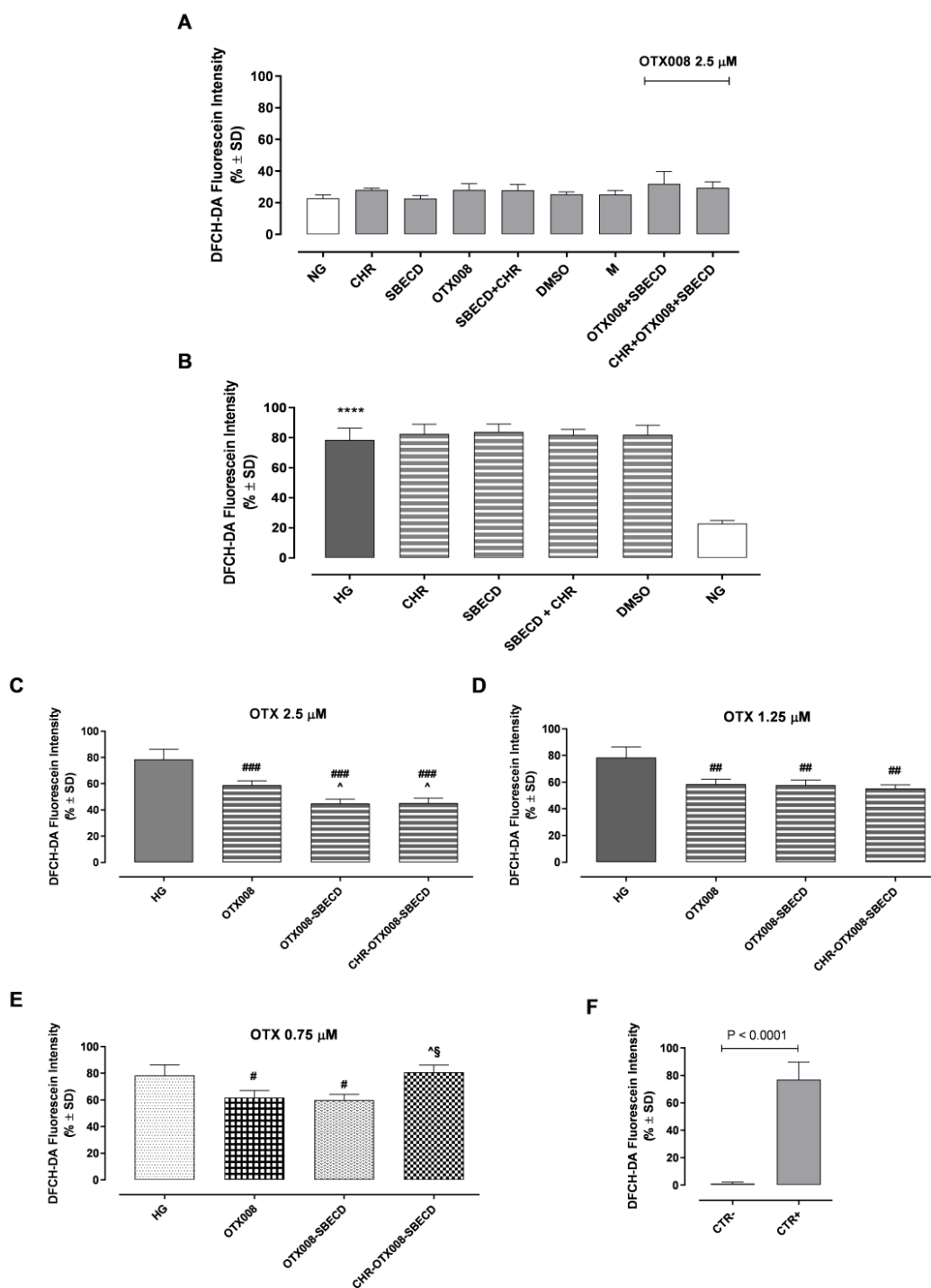


**Figure 9.** (A) 2',7'-dichlorodihydrofluorescein diacetate (DCFH-DA) levels in NG or (B) HG medium (where NG is reported as the control). In NG cells, OTX008 was tested at the maximum dose of 2.5 μM. In HG cells, OTX008 was tested at doses of 2.5–1.25–0.75 μM (C,D,E, respectively); (F) CTR− = negative control (5% FBS without DCFH-DA); CTR+ = positive control (H<sub>2</sub>O<sub>2</sub> 100 μM). DCFH-DA probe was used to assess ROS levels, quantified on a flow cytometer (Figure S19), and reported as DCFH-DA fluorescein intensity ± SD. NG = 5.5 mM D-glucose; HG = 33 mM D-glucose; CHR = CHR 0.399 mg/mL; SBECD = Sulfobutylated -β-cyclodextrin 7.3 m/m%; SBECD + CHR = SBECD + 0.095 mg/mL CHR; DMSO = dimethyl sulfoxide 2.5%; M = mannitol 27.5 mM; OTX008 = OTX008 (2.5–1.25–0.75 μM); OTX008-SBECD = OTX(2.5–1.25–0.75 μM)-SBECD; CHR-OTX008-SBECD = CHR (0.324 mg/mL)-OTX(2.5–1.25–0.75 μM)-SBECD. \*\*\*\* *p* < 0.0001 vs. NG; # *p* < 0.05, ## *p* < 0.01, ### *p* < 0.001 vs. HG; ^ *p* < 0.05 vs. OTX008; § *p* < 0.01 vs. OTX008-SBECD.

### 3. Discussion

Chronic hyperglycemia-induced fibrosis affects vascular structures, leading to diabetic complications like retinopathy and liver fibrosis [19]. This fibrogenic process involves inflammatory mediators, cytokines, and growth factors, especially TGF- $\beta$ . This leads to increased extracellular matrix deposition. Past research on the flavonoid CHR in rodents showed its antifibrotic effects. CHR counteracts fibrosis by inhibiting hepatic cell activation via the TGF- $\beta$ 1/Smad pathway [20]. Additionally, CHR adjusts extracellular matrix dynamics and reduces collagen synthesis [11].

Recent studies highlight the Gal-1 protein as a therapeutic target for diabetic fibrosis. Elevated Gal-1 levels were found in diabetic mice's kidneys, contributing to kidney fibrogenesis [21,22]. Additionally, OTX008 has proven effective in preventing Gal-1 accumulation and countering the effects of TGF- $\beta$  on ARPE-19 cells in high glucose situations [23].

In this study, we suggest the concurrent administration of CHR and OTX008 as a strategy to combat fibrosis. However, this approach requires an appropriate delivery system to facilitate their combined solubilization and delivery. SBECD was chosen as the preferred carrier due to its established safety for parenteral use, superior solubilizing capabilities, and polyanionic character [24–26]. Previous research has demonstrated the successful solubilization of CHR using SBECD [5]. The potential interaction between SBECD and OTX008 was inferred from their chemical structures. Subsequent solubilization tests and chemico-physical examinations confirmed that SBECD, OTX008, and CHR interact to create a ternary complex, with initial findings indicating that SBECD is capable of dissolving OTX008. Phase solubility tests of CHR clearly showed the difference between the solubilization mechanisms and the structure of the formed complexes in the binary CHR-SBECD and ternary CHR-OTX008-SBECD complexes. The positively skewed curve of the ternary complexes points to the fact that bigger molecular associates were formed and increased the solubility of CHR compared to SBECD. This phenomenon is well-known in the case of cyclodextrins [27]; however, in calixarene-cyclodextrin macrostructures, it is less studied. The solubility of CHR is pH-dependent; in the range of pH 6.20–9.40, the two OH groups of the molecule are ionizable, and the two ionizations take place, forming a dianion [28]. In accordance with our results, in the presence of SBECD, increasing the pH from 3.65 to 9.95 resulted in approximately a twofold increase in CHR solubility. SBECD-CHR host-guest interaction is favorable from computational calculations ( $-4.5 \text{ kcal mol}^{-1}$ ), also supported by the NMR data, with CHR accommodated inside the toroid cavity of the cyclodextrin ring. Molecular simulation revealed another interesting mechanism in the interaction of CHR and SBECD. The OH groups of CHR chemically interact with the sulfobutyl ether (SBE) pendant groups, which is not the conventional host-guest mechanism of cyclodextrins but can contribute to the solubilization of CHR. SBECD has an average of six SBE arms; thus, it can amplify the number of interactions with CHR molecules besides the host-guest interaction. The solubilization of OTX008 with SBECD resulted in an alkaline solution with a pH of 9.36; however, it increased the CHR solubility fourfold, showing that the interactions with OTX008 were required for significant CHR solubilization. In the ternary complex of CHR-OTX008-SBECD, the NMR signals of CHR's OHs are significantly changed, confirming the involvement of OH groups in the formation of ternary complexes. The signals of the amide group and aromatic rings of OTX008 are also modified, showing involvement in the interaction in the ternary complex. Indeed, the most preferential interactions are on the carbonyl and amine groups ( $-12.6 \text{ kcal mol}^{-1}$  and  $-10.8 \text{ kcal mol}^{-1}$ , respectively) of OTX008 with CHR.

The presented geometries and binding energies suggest that the experimentally enhanced entrapment of CHR with an OTX008-SBECD mixture is additive in nature, and the higher solubility observed can be justified by a combination of these mechanisms, leading to a supramolecular structure. The SBECD is able to bind at least 6 CHR molecules (one on each arm), with the potential for multiple CHR per  $\text{SO}_3^-$  moiety. Subsequently, the addition of OTX008 allows for 1:1 CHR-OTX008 adducts to be formed. The CHR is preferentially located within the amide arms (allowing for additional secondary interactions),

and optimization of an external amide interaction proves less stable, suggesting the 1:1 complex is most favored.

The hypothesis here is that the OH groups of CHR molecules located in position 7 (Figure 6A) are involved in hydrogen bonding with OTX008 molecules (CONH) and/or in interactions with the tails of SBECD to produce a supramolecular structure; the higher solubilization of the CHR in the ternary structure is due to the cooperation of three effects: i) electrostatic bonding of CHR with OTX008 and SBECD molecules acting as bridges, ii) inclusion of CHR molecules in the SBECD toroid and calixarene structures, and iii) entrapment of CHR molecules in the free volume of the new supramolecular structure, facilitated by the strong CHR–CHR binding energy (Figure 10). This high solubilization of CHR is strictly associated with this specific ternary system.

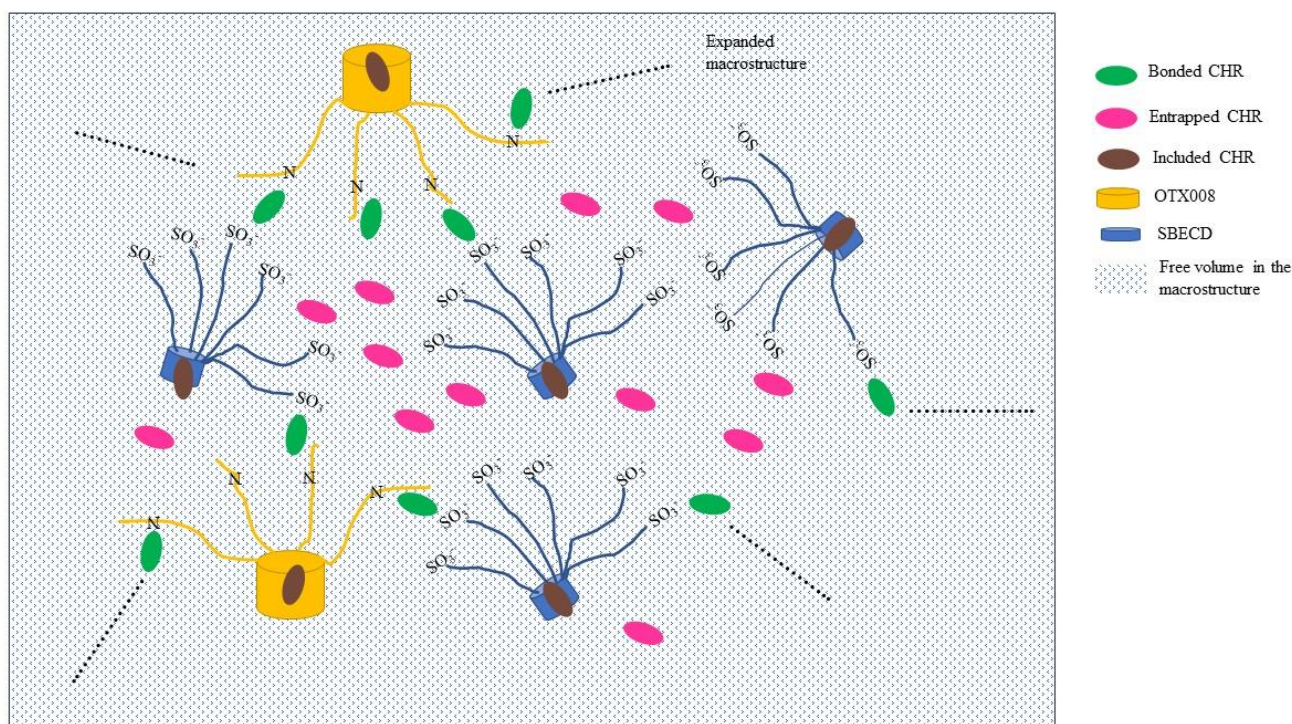


**Figure 10.** Schematic representation of the CHR-OTX008-SBECD macrostructure with CHR molecules making the link between SBECD and OTX008 molecules (green discs), dispersed in the free volume created in the macrostructure (purple discs), and trapped in the CD toroid or calixarene structure (brown discs). The synergy of the three situations enhances the CHR solubility in the ternary mixture.

Based on the phase solubility data and DLS results, large molecular associations are formed in the solution of OTX008 and SBECD (1002 nm, 86.8% intensity), which further increased after the solubilization of CHR (2698 nm, 75.2% intensity). Between the molecules that form the supramolecular associations, the free volume takes place [29,30], where CHR can be accumulated by the supramolecular structure. The special structure of the two association builder macrocycles, OTX008 and SBECD, helps the accumulation of CHR between macro chains or side groups. The structure supports the formation of the favored supramolecular carrier by binding free energies, complexation, and free volumes.

An attempted scheme with the proposed supramolecular structure is reported in Figure 10.

Finally, the biocompatibility of the complexes was tested on H9c2 (2-1) cells under normal and hyperglycemic conditions. The tested compounds alone, binary, and ternary complexes were not toxic to cells in NG or HG medium. Moreover, the binary and ternary complexes of OTX008 prevented the toxic effects of HG medium on H9c2 cells, especially

at the maximum dose of OTX008 (2.5  $\mu$ M), which was the most effective. The same trend was shown by the binary and ternary complexes of OTX008 in reducing intracellular ROS levels observed in H9c2 cells exposed to the HG condition. Building on our prior research that highlighted CHR's antifibrotic capabilities [11,20] and OTX008's intervention in the profibrotic Gal-1/TGF- $\beta$  pathway in a hyperglycemic environment [21], this newly devised drug delivery system, CHR-OTX008-SBECED, emerges as a promising candidate for modulating fibrotic progression associated with chronic diabetes. In this regard, its antifibrotic properties have been verified in H9c2 exposed to hyperglycemic conditions, while its safety and efficacy have been tested intraperitoneally in adult CD1 male mice with chronic diabetes. In this *in vivo* experimental setting, CHR-OTX008-SBECED led to a significant reduction in cardiac fibrosis markers and cardiac tissue remodeling without any toxicity by improving both CHR and OTX008 solubility in water and bioavailability [31]. Further detailed *in vitro* and *in vivo* studies are essential to discern the specific cellular and molecular mechanisms driving its therapeutic potential.

## 4. Materials and Methods

### 4.1. Materials

OTX008, known as Calixarene 0118, was obtained from Selleck Chemicals GmbH. The sulfobutylated  $\beta$ -cyclodextrin sodium salt (SBECED), with a degree of substitution (DS) around 6, was procured from Cyclolab Ltd. in Budapest, Hungary. CHR, chemically identified as 5,7-Dihydroxyflavone, was purchased from Alfa Aesar (by ThermoFisher Scientific in Kandel, Germany), while all other chemical reagents were supplied by Sigma.

### 4.2. Methods

#### 4.2.1. Solubilization Studies

##### OTX008 Solubilization with SBECED (Binary Systems)

SBECED solutions with increasing concentrations were prepared using ultrapure water (Millipore Direct-Q 5UV system, Merck Millipore, Burlington, MA, USA), and the same amounts of OTX008 were tested to dissolve in them to reveal the solubilization ability of SBECED on OTX008. OTX008 was clearly dissolved in the 7.3 m/m% SBECED solution at a 0.75 mg/mL final concentration to obtain the OTX008-SBECED solution.

##### CHR Solubilization in OTX008-SBECED Solution (Ternary Systems)

CHR was added in excess to solutions of OTX008-SBECED, prepared as per method 4.3.1, and agitated for 72 h at room temperature in closed vials ( $n = 3$ ). Post-incubation, the mixtures were centrifuged at 11,000 rpm for 10 min. The resulting clear supernatants were then separated, and the solubilized CHR concentration was determined using a UV spectrophotometer (Shimadzu UV-1900, Kyoto, Japan) at a wavelength of 270 nm. CHR solubilization was similarly conducted in the solution of 7.3 m/m% SBECED in the absence of OTX008, following the same incubation and preparation process.

The clarified CHR solutions were subsequently frozen at  $-110$  °C and lyophilized using a ScanVac CoolSafe freeze dryer (Labogene, Allerød, Denmark). The resulting complexes were preserved at  $-20$  °C for further experiments.

#### Phase-Solubility Study

Solutions of 7.3 m/m% SBECED and OTX008-SBECED were made and then diluted in a 96-well plate with ultrapure water. A surplus of CHR was added to each well. The plates were then sealed and agitated for 72 h at room temperature. After shaking, the samples were passed through a MultiScreen Solvintert 96 Well Filter Plate with a 0.45  $\mu$ m pore size, Poly(tetrafluoroethylene) membrane (PTFE) (Merck Millipore Ltd., Tullagreen, Ireland), using a MultiScreen Resist vacuum manifold (EMD Millipore Corporation, Burlington, MA, USA). The filtered, clear supernatants were transferred to a Greiner UV-Star<sup>®</sup> 96-well plate, and the absorbance was measured at 270 nm using a Thermo Fisher Multiskan Go microplate reader (Thermo Fisher, Waltham, MA, USA).

#### pH-Dependent CHR Solubility Determination

SBECD solutions at a concentration of 7.3 m/m% were prepared using a sodium acetate–acetic acid buffer at various pH levels (pH = 3.65; 5.75; 7.45; 9.95) and dispensed into a 96-well plate. An excess of CHR was then added to each well, the plate was sealed, and the solubility of CHR was assessed as described in Phase-Solubility study.

In a different experimental setup, the pH levels of the 7.3 m/m% SBECD and OTX008-SBECD solutions were adjusted to pH 8.64 with a 0.2 M sodium acetate solution and to pH 3.65 with 0.1 M HCl, respectively. Following these pH adjustments, the solubilization test for CHR was carried out as previously described.

#### 4.3. Scanning Electron Microscopy (SEM) Analysis

The lyophilized samples of complexes were crushed and mounted on a fixture with graphite-containing, double-sided adhesive tape. The pure raw materials were used without being crushed. The surface of the samples was not coated with gold before the SEM examination. A vacuum and low accelerating voltage of 5–15 kV were used during the investigation by a Hitachi Tabletop microscope (TM3030 Plus, Hitachi High-Technologies Corporation, Tokyo, Japan).

#### 4.4. Size Distribution Measurement of the Cyclodextrin Complexes with Dynamic Light Scattering (DLS)

The particle size distribution in solutions of 7.3 m/m% SBECD and OTX008-SBECD, both with CHR complexed after the phase solubility tests and without CHR, was measured using a Malvern Nano-ZS Zetasizer (Malvern Instruments, Malvern, UK).

#### 4.5. Nuclear Magnetic Resonance (NMR) Studies

$^1\text{H}$  and NOESY NMR characterization of CHR, SBECD, OTX008, binary systems CHR-SBECD, OTX008-SBECD, and ternary system CHR-OTX008-SBECD were performed using a Bruker Ascend 400 MHz spectrometer (Billerica, MA, USA) with a double resonance broadband probe, BBFO model, and the spectra recorded at ambient temperature in dimethylsulphoxide ( $\text{DMSO-d}_6$ ) and/or deuterated water ( $\text{D}_2\text{O}$ ) depending on the solubility of the materials (typical solutions of 10 mg/mL). Lyophilised mixtures CHR-SBECD, OTX008-SBECD, and CHR-OTX008-SBECD were used as described in Section 4.2.1. The solvent peaks were referenced to 2.5 ppm ( $\text{DMSO-d}_6$ ) and 4.7 ppm (HDO,  $\text{H}_2\text{O}$ ). Peak multiplicities were described as follows: singlet (s), multiplet (m), and broad (br).

#### 4.6. Differential Scanning Calorimetry (DSC) Studies

The melting temperature ( $T_m$ ) and degradation temperature ( $T_d$ ) of all components and their binary and ternary mixtures were determined by Differential Scanning Calorimetry (DSC; Mettler Toledo, DSC 30 STAR System) at a heating rate of  $10\text{ }^\circ\text{C min}^{-1}$  and under an inert  $\text{N}_2$  atmosphere.

#### 4.7. Computational Studies

All calculations were undertaken using the Orca 4.2.1 software package [32]. Initial geometry optimization for CHR, OTX008, and SBECD and all interaction variants was conducted with the GFN2-xtb semi-empirical quantum mechanical method [33]. The method has been shown to be robust for large-scale calculations (up to a few thousand atoms) of organic, organometallic, and biochemical systems. The inclusion of the D4 dispersion term makes GFN2-xtb ideal for studying structures involving non-covalent interactions [34].

To gain a more accurate energetic understanding of the molecular interactions, the structures were re-optimized with unconstrained Density Functional Theory (DFT) calculations using the RI-PBE(D3)/def2-svp level of theory [35–38], with subsequent solvated single point energy calculations at the RI-PBE(D3)/def2-tzvp level of theory [35–38] with the continuum solvent polarized method (cpcm), [39] simulating a water environment



(epsilon = 80.3). Analytical frequency calculations on the gas phase geometries were performed to account for enthalpic and entropic contributions to the free energy term, as well as to confirm all intermediates are true minima on the potential energy surface. Due to the scaling limitations of DFT and the focus on molecular interactions, the SBECD molecule was approximated by a single SBE arm when calculating the binding free energy for these interactions. A concentration-induced free-energy shift of  $RT \ln V_M = 1.89 \text{ kcal mol}^{-1}$  ( $V_M$ : molar volume of an ideal gas,  $T = 298 \text{ K}$ ) has been included to account for the shift from gas (1 atm) to solution (1 mol dm<sup>-3</sup>) phase.

#### 4.8. H9c2 Cell Culture

Embryonic rat cardiac H9c2 (2-1) cells (ECACC, Salisbury, UK) were cultured in Dulbecco's modified Eagle's medium (DMEM; Aurogene, Rome, Italy), containing 5.5 mM d-glucose and supplemented with 10% heat-inactivated fetal bovine serum (FBS; AU-S181H Aurogene, Rome, Italy), 1% L-Glutamine (L-Glu; AU-X0550 Aurogene, Rome, Italy), and 1% penicillin/streptomycin solution (P/S; AU-L0022 Aurogene, Rome, Italy), at 37 °C under an atmosphere of 5% CO<sub>2</sub>.

After reaching 80% confluence, H9c2 cells were trypsinized, seeded at a specific cell density for each assay, and then exposed to NG, high glucose (HG; 33 mM d-glucose), or NG + 27.5 mM mannitol (M; as an osmotic control) for 48 h [40]. Cells were then treated for 6 days [41] in NG or HG medium with the following substances:

- CHR 0.399 mg/mL (CHR), dissolved in NaCl;
- SBECD 7.3 m/m%, dissolved in NaCl;
- Binary system SBECD + 0.095 mg/mL CHR (SBECD + CHR), dissolved in NaCl;
- DMSO 2.5% as a vehicle of OTX008;
- OTX008 (0.75–1.25–2.50 μM);
- Binary system OTX008 (2.5–1.25–0.75 μM)-SBECD (OTX008-SBECD), dissolved in NaCl;
- Ternary system CHR (0.324 mg/mL)-OTX008 (2.5–1.25–0.75 μM)-SBECD (CHR-OTX008-SBECD), dissolved in NaCl.

Three independent experiments were conducted, each performed in triplicate (N = 9).

#### 4.9. Cell Viability Assay

H9c2 cells were plated at a density of  $1 \times 10^4$  cells per well in 96-well plates [42], exposed to NG or HG medium for 48 h, and then treated as described above.

At the end of the stimulation period, 3-(4,5-Dimethylthiazol-2-yl)-2,5-Diphenyltetrazolium Bromide (MTT) solution (1:10 in culture medium, 300 μL/well) was added to each well, incubated for 4 h at 37 °C, and then removed. Each well was then washed for 20 min with isopropanol-HCl 0.2 N. Optical density (OD) values were measured at 570 nm using a 96-well plate reader (iMark, Bio-Rad Laboratories, Segrate, Italy) [40].

#### 4.10. ROS Assessment

ROS levels were detected by the conversion of the fluorescent probe 2',7'-dichlorodihydrofluorescein diacetate (DCFH-DA) to highly fluorescent dichlorofluorescein (DFC) diacetate within cells by ROS. H9c2 cells were seeded in 6-well plates ( $5 \times 10^4$  cells/well) in NG or HG medium for 48 h and then treated as described above. At the end of the stimulation period, cells were loaded with 20 μM DCFH-DA in medium with 5% FBS at 37 °C for 30 min, then were trypsinized. Total intracellular ROS production was quantified on a Guava easyCyte flow cytometer (Merck Millipore, Burlington, MA, USA), following the manufacturer's instructions. Both cell types were exposed to medium 5% FBS without DCFH-DA as a negative control (CTR-) or incubated with H<sub>2</sub>O<sub>2</sub> (100 μM) for 30 min before trypsinization as a positive control (CTR+).

#### 4.11. Statistical Analysis

The results are reported as the mean  $\pm$  standard deviation (SD). Statistical significance was determined using a one-way analysis of variance (ANOVA), followed by Tukey's comparison test. A *p*-value less than 0.05 was considered significant to reject the null hypothesis.

### 5. Conclusions

Addressing fibrosis under hyperglycemic conditions remains a significant challenge, necessitating innovative approaches and therapeutic agents. In this study, we introduce a new ternary formulation and application of two potential drugs, namely CHR and OTX008 with SBECD, each targeting distinct pharmacological pathways within a Drug Delivery System (DDS) optimized for parenteral use. This marks the novel dual formulation of the calixarene derivative OTX008 and flavonoid CHR within a single DDS, where they uniquely and actively influence the structural formation of the resultant supramolecular ternary complex. Notably, OTX008 serves as a pivotal element of the ternary complex, both structurally and pharmacologically. Our findings suggest that the tailored ternary complex presents a novel and promising solution for the integrated treatment of fibrosis in hyperglycemic scenarios and can open a new chapter in the drug delivery of poorly water-soluble drugs.

**Supplementary Materials:** The following supporting information can be downloaded at: <https://www.mdpi.com/article/10.3390/ph17010107/s1>, Figure S1: Size distribution of the molecular associates of SBECD, OTX008-SBECD, and CHR-OTX008-SBECD in water; Figure S2:  $^1\text{H}$  NMR spectrum of OTX008 in DMSO- $d_6$ ; Figure S3:  $^1\text{H}$  NMR spectrum of SBECD in DMSO- $d_6$ ; Figure S4:  $^1\text{H}$  NMR spectrum of SBECD in  $\text{D}_2\text{O}$ ; Figure S5:  $^1\text{H}$  NMR spectra of CHR-SBECD mixture, CHR, and SBECD in DMSO- $d_6$ ; Figure S6:  $^1\text{H}$  NMR spectra of CHR-SBECD mixture and SBECD in  $\text{D}_2\text{O}$ ; Figure S7: NOESY NMR spectra of CHR, CHR-SBECD mixture, and SBECD in DMSO- $d_6$ ; Figure S8: Expanded area of the NOESY spectra Figure S7; Figure S9:  $^1\text{H}$  NMR spectra of OTX008-SBECD mixture, OTX008 and SBECD in DMSO- $d_6$ ; Figure S10: NOESY spectra of OTX008-SBECD mixture, OTX008 and SBECD in DMSO- $d_6$ ; Figure S11:  $^1\text{H}$  NMR spectra of CHR-OTX008-SBECD mixture, OTX008, SBECD, and CHR in DMSO- $d_6$ ; Figure S12: Expanded area of  $^1\text{H}$  NMR spectra of CHR-OTX008-SBECD mixture, OTX008, SBECD, and CHR in DMSO- $d_6$ ; Figure S13: Expanded area of  $^1\text{H}$  NMR spectra of CHR-OTX008-SBECD mixture, OTX008, SBECD, and CHR in DMSO- $d_6$ ; Figure S14: Expanded area of  $^1\text{H}$  NMR spectra of CHR-OTX008-SBECD mixture, OTX008, SBECD, and CHR in DMSO- $d_6$ ; Figure S15: Comparison of NOESY spectra of CHR, CHR-OTX008-SBECD mixture, and binary CHR-SBECD mixture in DMSO- $d_6$ ; Figure S16: NOESY spectra of the CHR-OTX008-SBECD mixture and SBECD in  $\text{D}_2\text{O}$ ; Figure S17: Zoomed view of DSC thermograms of CHR, OTX008, SBECD, and CHR-OTX008-SBECD; Figure S18: Comparison of zoomed areas of DSC thermograms of SBECD-OTX008 mixture, SBECD-CHR mixture, and CHR-SBECD-OTX008 mixture; Figure S19: Representative flow cytometer measures of total intracellular ROS levels assayed with the DCFH-DA probe; Figure S20: Interactions between SBECD and CHR, OTX008 and SBECD; Table S1: Results of thermal analysis.

**Author Contributions:** Conceptualization, A.H. (Anca Hermenean), E.D., A.H. (Alex Hamilton), M.D., and F.F.; methodology, A.H. (Anca Hermenean), E.D., A.H. (Alex Hamilton), M.C.T., M.R., Á.R., J.V., F.F., C.S., C.C.L., I.B. (Ildikó Bácskay), and I.B. (István Budai); investigation, E.D., A.H. (Alex Hamilton), M.C.T., M.R., Á.R., J.V., F.F., C.S., C.C.L., and I.B. (István Budai); resources, A.H. (Anca Hermenean); data curation, F.F.; writing—original draft preparation, A.H. (Anca Hermenean), E.D., A.H. (Alex Hamilton), F.F., Á.R., M.C.T., I.B. (Ildikó Bácskay), M.D., and J.V.; writing—review and editing, A.H. (Anca Hermenean), E.D., A.H. (Alex Hamilton), and F.F. All authors have read and agreed to the published version of the manuscript.

**Funding:** This work was supported by a grant from the Ministry of Research, Innovation, and Digitization, CNCS/CCCDI-UEFISCDI, project number PN-III-P4-ID-PCE-2020-1772, within PNCDDI III. Project no. TKP2021-EGA-18 has been implemented with the support provided by the Ministry of Culture and Innovation of Hungary from the National Research, Development, and Innovation Fund, financed under the TKP2021-EGA funding scheme. This work/publication is supported by

the GINOP-2.3.1-20-2020-00004 project. The project is co-financed by the European Union and the European Regional Development Fund.

**Institutional Review Board Statement:** Not applicable.

**Informed Consent Statement:** Not applicable.

**Data Availability Statement:** Data supporting this study are openly available from Cranfield's data repository (CORD) at this article.

**Conflicts of Interest:** The authors declare no conflicts of interest.

## References

1. Yu, G.; Chen, X. Host–guest chemistry in supramolecular theranostics. *Theranostics* **2019**, *9*, 3041–3074. [[CrossRef](#)] [[PubMed](#)]
2. Español, E.S.; Villamil, M.M. Calixarenes: Generalities and their role in improving the solubility, biocompatibility, stability, bioavailability, detection, and transport of biomolecules. *Biomolecules* **2019**, *9*, 90. [[CrossRef](#)] [[PubMed](#)]
3. Crini, G.; Fourmentin, S.; Fenyvesi, É.; Torri, G.; Fourmentin, M.; Morin-Crini, N. Cyclodextrins, from molecules to applications. *Environ. Chem. Lett.* **2018**, *16*, 1361–1375. [[CrossRef](#)]
4. Millership, J.S. A preliminary investigation of the solution complexation of 4-sulphonic calix[n]arenes with testosterone. *J. Incl. Phenom.* **2001**, *39*, 327–331. [[CrossRef](#)]
5. Fenyvesi, F.; Nguyen, T.L.P.; Haimho, Á.; Ruzsnyák, Á.; Vasvári, G.; Bácskay, I.; Vecsernyés, M.; Ignat, S.-R.; Dinescu, S.; Costache, M.; et al. Cyclodextrin Complexation Improves the Solubility. *Materials* **2020**, *13*, 3618. [[CrossRef](#)] [[PubMed](#)]
6. Cho, H.; Kim, K.; Kim, N.; Woo, M.; Kim, H.Y. Effect of propolis phenolic compounds on free fatty acid receptor 4 activation. *Food Sci. Biotechnol.* **2020**, *29*, 579–584. [[CrossRef](#)]
7. Rice-Evans, C.A.; Miller, N.J.; Paganga, G. Structure-antioxidant activity relationships of flavonoids and phenolic acids. *Free Radic. Biol. Med.* **1996**, *20*, 933–956. [[CrossRef](#)]
8. Birt, D.F.; Hendrich, S.; Wang, W. Dietary agents in cancer prevention: Flavonoids and isoflavonoids. *Pharmacol. Ther.* **2001**, *90*, 157–177. [[CrossRef](#)]
9. Ignat, S.; Dinescu, S.; Váradi, J.; Fenyvesi, F.; Nguyen, T.L.P.; Ciceu, A.; Hermenean, A.; Costache, M. Complexation with Random Methyl- $\beta$ -Cyclodextrin and (2-Hydroxypropyl)- $\beta$ -Cyclodextrin Promotes Chrysin Effect and Potential for Liver Fibrosis Therapy. *Materials* **2020**, *13*, 5003. [[CrossRef](#)]
10. Ciceu, A.; Balta, C.; Herman, H.; Gharbia, S.; Ignat, S.R.; Dinescu, S.; Váradi, J.; Fenyvesi, F.; Gyöngyösi, S.; Hermenean, A.; et al. Complexation with random methyl- $\beta$ -cyclodextrin and (2-hydroxypropyl)- $\beta$ -cyclodextrin enhances in vivo anti-fibrotic and anti-inflammatory effects of chrysin via the inhibition of NF- $\kappa$ B and TGF- $\beta$ 1/smad signaling pathways and modulation of hepatic pro/anti-f. *Int. J. Mol. Sci.* **2021**, *22*, 1869. [[CrossRef](#)]
11. Balta, C.; Ciceu, A.; Herman, H.; Rosu, M.; Boldura, O.M.; Hermenean, A. Dose-dependent antifibrotic effect of chrysin on regression of liver fibrosis: The role in extracellular matrix remodeling. *Dose-Response* **2018**, *16*, 1559325818789835. [[CrossRef](#)] [[PubMed](#)]
12. Bartocci, A.; Gillet, N.; Jiang, T.; Szczepaniak, F.; Dumont, E. Molecular dynamics approach for capturing calixarene–protein interactions: The case of cytochrome c. *J. Phys. Chem. B* **2020**, *124*, 11371–11378. [[CrossRef](#)] [[PubMed](#)]
13. Astorgues-Xerri, L.; Riveiro, M.E.; Tijeras-Raballand, A.; Serova, M.; Rabinovich, G.A.; Bieche, I.; Vidaud, M.; de Gramont, A.; Martinet, M.; Cvitkovic, E.; et al. OTX008, a selective small-molecule inhibitor of galectin-1, downregulates cancer cell proliferation, invasion and tumour angiogenesis. *Eur. J. Cancer* **2014**, *50*, 2463–2477. [[CrossRef](#)]
14. Zucchetti, M.; Bonezzi, K.; Frapolli, R.; Sala, F.; Borsotti, P.; Zangarini, M.; Cvitkovic, E.; Noel, K.; Ubezio, P.; Giavazzi, R.; et al. Pharmacokinetics and antineoplastic activity of galectin-1-targeting OTX008 in combination with sunitinib. *Cancer Chemother. Pharmacol.* **2013**, *72*, 879–887. [[CrossRef](#)] [[PubMed](#)]
15. Al-Obaidi, N.; Mohan, S.; Liang, S.; Zhao, Z.; Nayak, B.K.; Li, B.; Sriramarao, P.; Habib, S.L. Galectin-1 is a new fibrosis protein in type 1 and type 2 diabetes. *FASEB J.* **2019**, *33*, 373–387. [[CrossRef](#)] [[PubMed](#)]
16. Yang, W.; de Villiers, M.M. Effect of 4-Sulphonato-Calix[n]Arenes and cyclodextrins on the solubilization of niclosamide, a poorly water soluble anthelmintic. *AAPS J.* **2005**, *7*, 241–248. [[CrossRef](#)] [[PubMed](#)]
17. Ramesh, P.; Reddy, C.S.; Suresh Babu, K.; Reddy, P.M.; Srinivasa Rao, V.; Parthasarathy, T. Synthesis, characterization and molecular docking studies of novel 2-amino 3-cyano pyrano [2,3H]chrysin derivatives as potential antimicrobial agents. *Med. Chem. Res.* **2015**, *24*, 3696–3709. [[CrossRef](#)]
18. Song, S.; Gao, K.; Niu, R.; Wang, J.; Zhang, J.; Gao, C.; Yang, B.; Liao, X. Inclusion complexes between chrysin and amino-appended  $\beta$ -cyclodextrins (ACDs): Binding behavior, water solubility, in vitro antioxidant activity and cytotoxicity. *Mater. Sci. Eng. C* **2020**, *106*, 110161. [[CrossRef](#)]
19. Ban, C.R.; Twigg, S.M. Fibrosis in diabetes complications: Pathogenic mechanisms and circulating and urinary markers. *Vasc. Health Risk Manag.* **2008**, *4*, 575–596. [[CrossRef](#)]
20. Balta, C.; Herman, H.; Boldura, O.M.; Gasca, I.; Rosu, M.; Ardelean, A.; Hermenean, A. Chrysin attenuates liver fibrosis and hepatic stellate cell activation through TGF- $\beta$ /Smad signaling pathway. *Chem. Biol. Interact.* **2015**, *240*, 94–101. [[CrossRef](#)]

21. Kuo, C.S.; Chou, R.H.; Lu, Y.W.; Tsai, Y.L.; Huang, P.H.; Lin, S.J. Increased circulating galectin-1 levels are associated with the progression of kidney function decline in patients undergoing coronary angiography. *Sci. Rep.* **2020**, *10*, 1435. [[CrossRef](#)] [[PubMed](#)]
22. Liu, Y.; Long, L.; Yuan, F.; Liu, F.; Liu, H.; Peng, Y.; Sun, L.; Chen, G. High glucose-induced Galectin-1 in human podocytes implicates the involvement of Galectin-1 in diabetic nephropathy. *Cell Biol. Int.* **2015**, *39*, 217–223. [[CrossRef](#)] [[PubMed](#)]
23. Trotta, M.C.; Petrillo, F.; Gesualdo, C.; Rossi, S.; Della Corte, A.; Váradi, J.; Fenyvesi, F.; D’Amico, M.; Hermenean, A. Effects of the Calix[4]arene Derivative Compound OTX008 on High Glucose-Stimulated ARPE-19 Cells: Focus on Galectin-1/TGF- $\beta$ /EMT Pathway. *Molecules* **2022**, *27*, 4785. [[CrossRef](#)]
24. Stella, V.J.; Rajewski, R.A. Sulfobutylether- $\beta$ -cyclodextrin. *Int. J. Pharm.* **2020**, *583*, 119396. [[CrossRef](#)]
25. Pardeshi, C.V.; Kothawade, R.V.; Markad, A.R.; Pardeshi, S.R.; Kulkarni, A.D.; Chaudhari, P.J.; Longhi, M.R.; Dhas, N.; Naik, J.B.; Surana, S.J.; et al. Sulfobutylether- $\beta$ -cyclodextrin: A functional biopolymer for drug delivery applications. *Carbohydr. Polym.* **2023**, *301*, 120347. [[CrossRef](#)]
26. Luke, D.R.; Tomaszewski, K.; Damle, B.; Schlamm, H.T. Review of the Basic and Clinical Pharmacology of Sulfobutylether- $\beta$ -Cyclodextrin (SBECD). *J. Pharm. Sci.* **2010**, *99*, 3291–3301. [[CrossRef](#)] [[PubMed](#)]
27. Jansook, P.; Kurkov, S.V.; Loftsson, T. Cyclodextrins as solubilizers: Formation of complex aggregates. *J. Pharm. Sci.* **2010**, *99*, 719–729. [[CrossRef](#)] [[PubMed](#)]
28. Castro, G.T.; Ferretti, F.H.; Blanco, S.E. Determination of the overlapping pKa values of chrysin using UV-vis spectroscopy and ab initio methods. *Spectrochim. Acta—Part A Mol. Biomol. Spectrosc.* **2005**, *62*, 657–665. [[CrossRef](#)]
29. Sharma, J.; Tewari, K.; Arya, R.K. Diffusion in polymeric systems—A review on free volume theory. *Prog. Org. Coatings* **2017**, *111*, 83–92. [[CrossRef](#)]
30. Ramesh, N.; Davis, P.K.; Zielinski, J.M.; Danner, R.P.; Duda, J.L. Application of free-volume theory to self diffusion of solvents in polymers below the glass transition temperature: A review. *J. Polym. Sci. Part B Polym. Phys.* **2011**, *49*, 1629–1644. [[CrossRef](#)]
31. Trotta, M.C.; Herman, H.; Ciceu, A.; Mladin, B.; Rosu, M.; Lepre, C.C.; Russo, M.; Bácskay, I.; Fenyvesi, F.; Marfella, R.; et al. Chrysin-based supramolecular cyclodextrin-calixarene drug delivery system: A novel approach for attenuating cardiac fibrosis in chronic diabetes. *Front. Pharmacol.* **2023**, *14*, 1332212. [[CrossRef](#)] [[PubMed](#)]
32. Neese, F. Software update: The ORCA program system, version 4.0. *Wiley Interdiscip. Rev. Comput. Mol. Sci.* **2018**, *8*, e1327. [[CrossRef](#)]
33. Bannwarth, C.; Ehlert, S.; Grimme, S. GFN2-xTB—An Accurate and Broadly Parametrized Self-Consistent Tight-Binding Quantum Chemical Method with Multipole Electrostatics and Density-Dependent Dispersion Contributions. *J. Chem. Theory Comput.* **2019**, *15*, 1652–1671. [[CrossRef](#)]
34. Caldeweyher, E.; Bannwarth, C.; Grimme, S. Extension of the D3 dispersion coefficient model. *J. Chem. Phys.* **2017**, *147*, 034112. [[CrossRef](#)]
35. Neese, F. An Improvement of the Resolution of the Identity. *J. Comput. Chem.* **2003**, *24*, 1740–1747. [[CrossRef](#)] [[PubMed](#)]
36. Perdew, J.P.; Burke, K.; Ernzerhof, M. Generalized gradient approximation made simple. *Phys. Rev. Lett.* **1996**, *77*, 3865–3868. [[CrossRef](#)]
37. Weigend, F.; Ahlrichs, R. Balanced basis sets of split valence, triple zeta valence and quadruple zeta valence quality for H to Rn: Design and assessment of accuracy. *Phys. Chem. Chem. Phys.* **2005**, *7*, 3297–3305. [[CrossRef](#)]
38. Grimme, S.; Ehrlich, S.; Goerigk, L. Effect of the damping function in dispersion corrected density functional theory. *J. Comput. Chem.* **2011**, *32*, 1456–1465. [[CrossRef](#)]
39. Barone, V.; Cossi, M. Conductor Solvent Model. *J. Phys. Chem. A* **1998**, *102*, 1995–2001. [[CrossRef](#)]
40. Trotta, M.C.; Maisto, R.; Alessio, N.; Hermenean, A.; D’Amico, M.; Di Filippo, C. The melanocortin MC5R as a new target for treatment of high glucose-induced hypertrophy of the cardiac H9c2 cells. *Front. Physiol.* **2018**, *9*, 1475. [[CrossRef](#)]
41. Ghosh, R.; Hwang, S.M.; Cui, Z.; Gilda, J.E.; Gomes, A.V. Different effects of the nonsteroidal anti-inflammatory drugs meclofenamate sodium and naproxen sodium on proteasome activity in cardiac cells. *J. Mol. Cell. Cardiol.* **2016**, *94*, 131–144. [[CrossRef](#)] [[PubMed](#)]
42. Peng, Z.; Zhang, R.; Pan, L.; Pei, H.; Niu, Z.; Wang, H.; Lv, J.; Dang, X. Glucocalyxin A Protects H9c2 Cells Against Hypoxia/Reoxygenation-Induced Injury Through the Activation of Akt/Nrf2/HO-1 Pathway. *Cell Transplant.* **2020**, *29*, 0963689720967672. [[CrossRef](#)] [[PubMed](#)]

**Disclaimer/Publisher’s Note:** The statements, opinions and data contained in all publications are solely those of the individual author(s) and contributor(s) and not of MDPI and/or the editor(s). MDPI and/or the editor(s) disclaim responsibility for any injury to people or property resulting from any ideas, methods, instructions or products referred to in the content.